Molecular Weight Dependence of Chain Packing and Semicrystalline Structure in Oriented Films of Regioregular Poly(3-hexylthiophene) Revealed by High-Resolution Transmission Electron Microscopy

Martin Brinkmann*,† and Patrice Rannou‡

Institut Charles Sadron, 23 Rue du Loess, 67083 Strasbourg, France, and Laboratoire d'Electronique Moléculaire, Organique et Hybride, UMR5819-SPrAM (CEA/CNRS/Univ. J. FOURIER-Grenoble I), INAC, CEA-Grenoble, 17 Rue des Martyrs, F-38054 Grenoble Cedex 9, France

Received October 17, 2008; Revised Manuscript Received December 18, 2008

ABSTRACT: The semicrystalline structure of regioregular head-to-tail- (HT-) coupled poly(3-hexylthiophene-2,5-diyl) (Rr-P3HT) thin films grown by directional epitaxial solidification (DES) has been studied by high-resolution transmission electron microscopy (HR-TEM). A 10-fold increase of the weight-average molecular weight of the Rr-P3HT leads to several major structural changes: (i) an increase of the fluctuations of the lamellar thickness while preserving the average length of the polymer stems in the crystalline domains; (ii) an increase of the disorder in the crystalline packing of Rr-P3HT chains; (iii) an enhanced interconnectivity between crystalline lamellae via tie-crystallites and tie-chains; (iv) for $M_w \geq 18.8$ kDa equiv PS, preferential tilt angles of the polymer chains in the crystalline lamellae. Similar to stiff-chain polymers like poly(etheretherketone), the concomitant increase of the interchain distance (i.e., the *a* parameter in the unit cell) and the tilting of Rr-P3HT chains in the crystalline lamellae are attributed to chain folding exerting stress on the crystal packing because of the stiffness of comb-shaped Rr-P3HT chains.

1. Introduction

π-conjugated homopolymers like regioregular head-to-tail (HT)-coupled poly(3-alkylthiophene-2,5-diyl)s (Rr-P3ATs)[1] or poly(9,9-dialkylfluorene-2,7-diyl)[2,3] are archetypal polymeric semiconductors (PSCs) for the elaboration of low-cost and large-area organic electronic devices[4] viz. polymer field-effect transistors (PFETs)[5−11] and bulk-heterojunction polymeric solar cells.[12−20] Rr-P3ATs are benchmark PSCs widely used to prepare PFETs with high charge carrier mobilities up to *ca.* $10^{-2}-10^{-1}$ cm^2/V•s.[5−11,21] Electrical performances of the PFETs depend on a large palette of entangled factors such as the following: (i) PSCs intrinsic characteristics (chemical purity[1,7,22] (e.g., type and degree of regioregularity for Rr-P3ATs), macromolecular parameters[7,11,21,23−27] (i.e., weight-average M_w and number-average M_n molecular weights and polydispersity index $I = M_w/M_n$), (ii) processing conditions of the thin film (e.g., solvent used for the spin coating, solvent or thermal annealing procedures[28−30]), and (iii) quality of the PSC/gate dielectric interface which controls the efficiency of the charge transport.[31−34]

Several groups have recently observed that the charge carrier mobility of Rr-P3HT thin films in PFET configurations tends to increase with increasing molecular weight of Rr-P3HT.[7,11,21,23−27] This increase in charge carrier mobility has been attributed to the observed modifications of the thin film structure and morphology. Therefore, understanding the origin of the molecular weight dependence of the charge transport properties in Rr-P3ATs has to take into account the semicrystalline nature of this class of semiconducting polymer, i.e., the fact that both crystalline domains and amorphous zones coexist in the polymer films. Given the difference in charge mobility expected for crystalline and amorphous domains, it is of pivotal importance to uncover the interconnectivity between the crystalline zones. Crystalline and amorphous domains in Rr-P3ATs can be recognized by transmission electron microscopy (TEM) in the bright field and dark field modes on oriented thin films grown by the directional epitaxial solidification (DES) technique.[35,36] TEM investigations on epitaxied thin films revealed the periodic alternation of crystalline lamellae and amorphous interlamellar zones for various Rr-P3ATs. However, in the bright field (BF) mode used in refs 35 and 36, the distinction between crystalline and amorphous domains was based on the "defocus contrast" which does not provide a direct vizualization of polymer chain arrangements in the crystalline lamellae. In order to better understand the complex charge transport processes in Rr-P3HT thin films,[7,11] a detailed observation of the morphology of the active layer at the length scale of polymer chains is highly desirable.

Direct access to the chain packing in Rr-P3HT films can be obtained by scanning tunneling microscopy (STM) on (sub)-monolayers to a few monolayers thick films grown on HOPG substrates. Mena-Osteriz et al.[37] and Grévin et al.[38] have evidenced chain folding for various Rr-P3ATs grown on HOPG by STM and proposed molecular models showing that the succession of 3-*n*-alkylthiophene units in *cis* conformation can account for the formation of tight hairpin folds.[37,38] Also, grazing-incident X-ray diffraction studies on *ca.* sub-200 nm thick samples have yielded valuable structural information since this technique allows to probe the structure of the Rr-P3HT films from the free polymer surface down to the buried PSC/dielectric interface.[27,31] Several groups have clearly evidenced the impact of M_w on the unit cell parameters of Rr-P3HT in spin-coated thin films but the precise semicrystalline structure could not be analyzed directly by this method.[23−31]

The important results obtained by STM on Rr-P3ATs bear two main limitations: (i) they concern films with a thickness of at most *a few monolayers*, and (ii) the growth is performed on (semi)conducting substrates (e.g., HOPG). Specific interactions between Rr-P3HT chains and the substrate can induce peculiar growth patterns which may or may not be representative of the complex structure observed in the Rr-P3HT layers grown on dielectric substrates (e.g., oxides like SiO_2, Al_2O_3, HfO_2, self-assembled monolayers, etc.).

* Corresponding author.
† Institut Charles Sadron.
‡ Laboratoire d'Electronique Moléculaire, Organique et Hybride, UMR5819-SPrAM (CEA/CNRS/Univ. J. FOURIER-Grenoble I), INAC, CEA-Grenoble.

10.1021/ma8023415 CCC: $40.75
Published on Web 01/30/2009

Table 1. Macromolecular SEC Parameters (M_n, M_w and $I = M_w/M_n$) and Structural Characteristics (L_p, L_{cryst}, L_{lam}, and L_a) Obtained from HR-TEM Measurements on Oriented Rr-P3HT Films Obtained by DES of the Low-M_w, Medium-M_w, and High-M_w Fractions

	M_n [kDa equiv PS]	M_w [kDa equiv PS]	$I = M_w/M_n$	L_p[a] [nm]	L_{cryst} [nm]	L_{lam} [nm]	L_a (polymer stems)
low-M_w	5.7	7.3	1.3	9	7.5	11.5	20−25
medium-M_w	11.0	18.8	1.7	14	9.1	28	10−20
high-M_w	34.3	69.6	2.0	30	8.7	25	10−20

[a] The average length of the fully extended Rr-P3HT chains (in all-trans conformation) L_p was calculated by taking into account the corrected M_n values using the correction factors obtained from Figure 4 in ref 41 and an inter-3HT units distance of 0.38 nm.

In contrast to STM, *HR-TEM* can provide 2D projections of the polymeric chain arrangement in single-crystalline domains and oriented thin films with a thickness up to ca. 100 nm.[39] If the electron beam is parallel to a given crystallographic direction, e.g. parallel to the polymer stems, HR-TEM can give detailed informations on packing defects (dislocations), twinning and polymorphism in molecular materials and polymers.[39,40] However, the observation of chain packing in semicrystalline polymer films of polyolefins and polyesters is limited by their high sensitivity to the electron beam. To minimize the damage of the sample by the electron beam, it is necessary to work with low irradiation levels (typically below 400 electrons/nm^2 at 200 kV for a polymer like poly(tetramethyl-*p*-silphenylene siloxane).[40]

In this present study, we present direct observations of the chain packing and the semicrystalline structure of Rr-P3HT samples with different molecular weights using HR-TEM on P3HT thin films grown by DES.[35,36] As demonstrated hereafter, the increase of M_w affects mainly the extension of crystalline domains vs amorphous interlamellar zones, the tilt of the chains in the crystalline lamellae and the connectivity between crystalline domains. These effects will be discussed in terms of chain folding.

2. Experimental Section

Two commercial batches of regioregular HT-coupled poly(3-hexylthiophene-2,5-diyl) were obtained from Merck (Rr-P3HT with an HT-HT triad content> 96%) and Aldrich (Rr-P3HT with an HT-HT triad content> 99%). While the as-received P3HT sample from Merck, termed hereafter P3HT-medium-M_w-1 was used as received, the Aldrich P3HT batch consists of a mixture of oligomeric and polymeric species as demonstrated by its polydispersity index value of *ca.* 2.10. Fractionation (Soxhlet extraction) was used in order to obtain purified fractions with narrower polydispersity index values and well-defined molecular weights. To do so, a sequence of four solvents was used: acetone, *n*-hexane, CH_2Cl_2, and THF. The fraction of the lowest molecular weight (i.e., the acetone one) was discarded while the *n*-hexane, CH_2Cl_2, and THF fractions, hereafter labeled as P3HT-low-M_w, P3HT-medium-M_w-2, P3HT-high-M_w, were collected and studied in comparison with the so-called "P3HT-Low-M_w-1" one. Given the similar characteristics of the P3HT-Medium-M_w-2 and P3HT-medium-M_w-1 samples, the present study was restricted to the P3HT-medium-M_w-1 sample. The corresponding size exclusion chromatography (SEC) macromolecular parameters (M_n, M_w, and $I = M_w/M_n$) are given in ref 36. In the discussion of section 3, we have corrected the molecular weights determined by SEC using the correction factors in the range 1.2−2.6 obtained from the graph showing the relationship between M_n obtained by SEC and MALDI data in ref 41. Table 1 collects the structural and the macromolecular parameters of the samples used herein.

The oriented thin films of Rr-P3HT were grown by directional epitaxial solidification (DES)[35,36] in 1,3,5-trichlorobenzene (TCB). The detailed methodology for the preparation of the oriented films is given in refs 35 and 36. The film thicknesses (in the 10−50 nm range) were determined by atomic force microscopy (Nanoscope III in tapping mode using Si tips (25−50 N/m and 280−365 kHz)). The Rr-P3HT films were coated with a thin amorphous carbon film. Areas of interest in the oriented films were identified under a polarized optical microscope (Leica DMR-X microscope). The P3HT/carbon films were removed from the glass substrate by floating the samples on a 5 wt % aqueous HF solution and were subsequently recovered onto TEM copper grids. The TEM studies were performed with a CM12 Philips microscope (120 kV) equipped with a MVIII (Soft Imaging System) CCD camera. The high resolution images were acquired in a modified low-dose mode as explained hereafter. First, focusing and astigmatism corrections were performed on a test area, then the electron beam was blanked and the sample position was shifted to an unexposed nearby area. Stabilization of the mechanical drifts of the sample was observed after *ca.* 30−40 s. The numerical images (1376 × 1032 pixels) were acquired at 230k magnification, with a beam current <10 pA/cm^2 and an exposure time of *ca.* 0.5−1.0 s. Image analysis (Fast-Fourier Transform (FFT) and image filtering) was performed by using the AnalySIS (Soft Imaging System) software. The contrast between crystalline and amorphous areas of the polymer in the images was enhanced by using a Bragg filter on the FFT (see Supporting Information S1). Particular care was taken to avoid introducing artifacts in the HRTEM images upon filtering. Typically, the radius of the Bragg window was set to a value of 136 pixels for an image of total size 1024 × 1024 pixels. As seen in Figure S1, no artifacts like the formation of a ghost lattice in the amorphous interlamellar zones is observed.[42] Molecular modeling was performed on a Silicon Graphics station with the Cerius^2 software (Accelrys Ltd., Cambridge, U.K.).

3. Results and Discussions

3.1. Evolution of the Semicrystalline Structure with Increasing M_w. As demonstrated in our previous study,[36] the oriented films of low-M_w P3HT exhibit a peculiar morphology with the formation of two distinct types of oriented domains on the TCB substrate, namely "*flat-on*" and "*edge-on*" lamellae.[43] These two types of oriented crystalline P3HT lamellae are seen in the underfocused BF of Figure 1a. In Figure 1b, we show a low-dose HR-TEM image corresponding to a similar zone. The two type of domains observed in the defocused BF image of Figure a can also be observed in the HR-TEM image. We have depicted the packing of two polymeric chains in the unit cell in Figure 1c and the chain packing within the edge-on and flat-on crystalline domains in Figure 1d.[44] For both types of domains, we find the same *interchain* periodicity of 1.57 ± 0.03 nm (as determined from the FFT), which corresponds to the distance between P3HT chains separated by layers of *n*-hexyl side-chains, i.e., to the *a* axis of the monoclinic unit cell determined by electron diffraction in reference[36] ($a = 1.6$ nm, $b = 0.78$ nm, $c = 0.78$ nm and $\gamma = 93.5°$). For edge-on crystalline lamellae, the observed contrast in the HR-TEM image is ascribed to the succession of the π-stacked polythiophene-stiff backbones in the (*b,c*) planes which contain the electron-rich sulfur atoms and the layers of *n*-hexyl side chains. The main difference between edge-on and flat-on lamellae lies in the contrast which is more pronounced for the edge-on oriented lamellae. This difference in contrast reflects the different

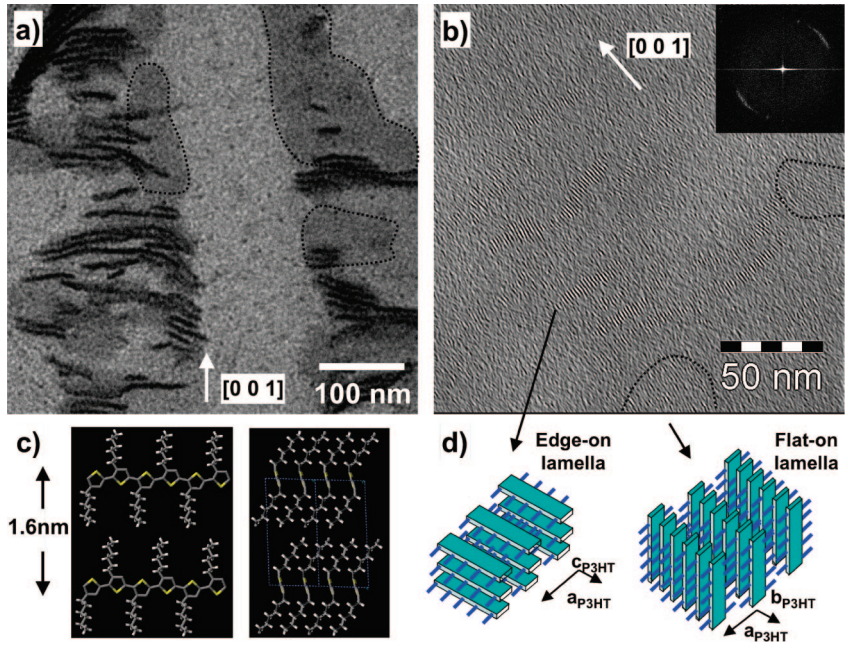

Figure 1. (a) Underfocused BF TEM image of a thin area of an oriented thin film of Rr-P3HT with M_w = 7.3 kDa equiv PS grown by DES.[35,36] The flat-on lamellae have been delimitated by a dotted line. (b) Low-dose HR-TEM image. The flat-on lamellae have been identified by a dotted line. The average in-plane chain orientation is indicated by a white arrow. The inset corresponds to the FFT. (c) Schematic representation of the chain packing of P3HT seen along the *b* and *c* axis.[44] (d) Scheme showing the chain orientation in flat-on and edge-on lamellae seen in the HR-TEM image.

orientations of the P3HT chains in edge-on and flat-on lamellae (see Figure 1.d) as well as the difference in the thicknesses of the ordered domains. Whereas the edge-on lamellae have a thickness of *ca.* 20−50 nm (as obtained from AFM measurements), flat-on lamellae have thicknesses corresponding to the lamellar periodicity of the P3HT low-M_w sample i.e. 10−12 nm (*vide infra*). As demonstrated previously by using the dark field method, the HR-TEM image in Figure 1.b indicates that edge-on and flat-on lamellae share the same in-plane orientation of the **a** axis as a consequence of epitaxial growth conditions of Rr-P3HT on TCB.[36]

The edge-on crystalline lamellae have a thickness L_{cryst} of *ca.* 6−7 nm corresponding to *ca.* 15−18 units of 3-*n*-hexylthiophene (3HT) vs an extended corrected chain length of 23 3-*n*-hexylthiophene units (3HT).[41] The total periodicity of the semicrystalline structure (i.e., a crystalline lamella plus an amorphous interlamellar zone) amounts to 10−12 nm, in good agreement with the interlamellar distance in the underfocused BF image (Figure 1a). Both the underfocused BF TEM image (Figure 1a.) and the low-dose HR-TEM image (Figure 1b) point at the existence of relatively narrow 4−5 nm-thick amorphous interlamellar zones.

Contrary to certain π-conjugated polymers, e.g., poly(nonylbithiazole), we do not observe substantial curvature and lattice bending within the crystalline ordered domains of Rr-P3HT.[45] This difference is ascribed to the epitaxial orientation of Rr-P3HT on the TCB substrate which determines the in-plane chain orientation of Rr-P3HT.

In Figure 2 we depict the defocused BF TEM image and the low dose HR-TEM image of an oriented Rr-P3HT film for M_w = 18.8 kDa equiv PS. Figure 3 shows different low-dose HR-TEM images corresponding to different interesting areas in the oriented films of the high-M_w sample with M_w = 69.9 kDa equiv PS. The increase of M_w results in important changes of the semicrystalline structure of the oriented Rr-P3HT films. As for the low-M_w sample, a periodic alternation of crystalline domains corresponding to the edge-on lamellae and rather extended disordered interlamellar zones is evidenced for $M_w \geq$ 18.8 kDa

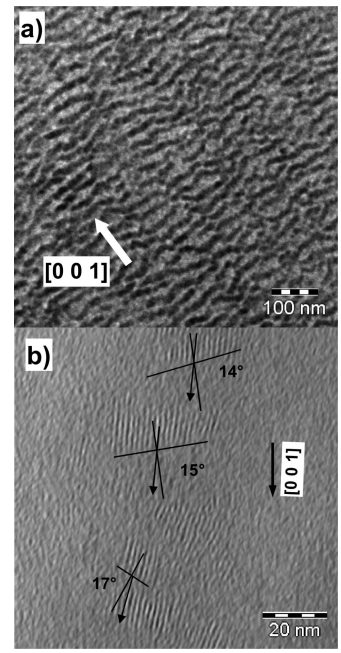

Figure 2. (a) Underfocused BF TEM image of a thin area of an oriented thin film of Rr-P3HT with M_w = 18.8 kDa equiv PS grown by DES.[35,36] (b) Low-dose HR-TEM image of an equivalent area showing the crystalline lamellae of P3HT with edge-on orientation. The edge of the crystalline lamellae is indicated by a line and the average chain orientation in the lamellae by an arrow. The average in-plane orientation of the chain axis is also indicated by an arrow.

equiv PS. However, the comparison with the low-M_w sample reveals several interesting differences which affect mainly: (i) the crystalline order within the lamellae, (ii) the extension of the amorphous interlamellar zones, (iii) the connectivity between crystalline domains, and (iv) the tilting of the Rr-P3HT chains in the crystalline lamellae.

Let us first focus on the impact of increasing M_w on the size of the crystalline domains of Rr-P3HT. Due to the strong

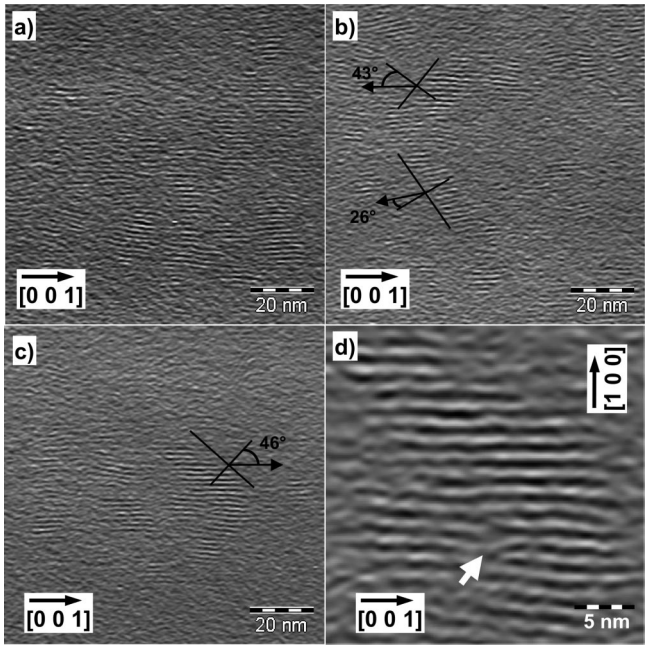

Figure 3. Low-dose HR-TEM images of various representative areas showing edge-on crystalline domains in a DES-oriented[35,36] high-M_w Rr-P3HT thin film. The polymer is characterized by a M_w value of 69.6 kDa equiv PS. In parts b and c, the black arrow show the stem orientation in the crystalline lamellae and the full line depicts the edge of some crystalline domains. In part d, the white arrow points at a structural defect at the junction between two lamellar crystals. The defect corresponds most likely to an edge dislocation. Note the fluctuations of the interchain distance between successive rows of π-stacked Rr-P3HT chains close to the defect which points at a certain plasticity of the Rr-P3HT crystal.

fluctuations of the lamellar thickness for samples with $M_w \geq$ 18.8 kDa equiv PS, possibly due to the high polydispersity of the samples (>1.7), the average thickness of the crystalline lamellae, L_{cryst}, was determined by a statistical measurement of the polymer stem length in the crystalline domains. The statistics was made over an average of 150−180 stems. The average stem length amounts to ca. 9.1 ± 0.5 nm for the medium-M_w sample and 8.7 ± 0.5 nm for the high-M_w sample. The fact that all three samples exhibit a similar crystalline lamellar thickness suggests that L_{cryst} does not scale with M_w. The increase in the total lamellar thickness, L_{lam}, (amorphous plus crystalline), between 11 nm for the low-M_w sample and 25−28 nm for the samples with $M_w \geq$ 18.8 kDa equiv PS results essentially from the increase of the thickness of the amorphous interlamellar zones which reaches a value of *ca.* 16−20 nm for $M_w \geq$ 18.8 kDa equiv PS.

The extension of crystalline order within the lamellae in the direction perpendicular to the chain axis (i.e., along the ***a*** axis) shows also some dependence on M_w. As noticed in our earlier study,[36] the crystalline lamellae of the low-M_w sample are remarkably uniform in thickness. In average, the persistence length of crystalline order along the **a** axis, L_a, corresponds to 20−25 polymer stems, i.e., a lateral crystallite size of ∼ 50 nm. For $M_w \geq$ 18.8 kDa equiv PS, the observed order along the **a** axis is reduced to 10−20 stems. The low-M_w lamellae grow with a preferential (0 1 0) contact plane on TCB whereas the samples with $M_w \geq$ 18.8 kDa equiv PS are characterized by a fiber-like orientation;[35,36] i.e., only some parts of the crystalline lamellae have their *b* axis collinear to the electron beam and show accordingly the proper (0 1 0) projection of the chain packing.

A further major difference between the samples concerns the connectivity between crystalline domains. As a matter of fact, for the low-M_w sample, the lamellar domains are always clearly separated by amorphous interlamellar zones and there is no evidence for ordered connecting paths between successive crystalline lamellae. For $M_w \geq$ 18.8 kDa equiv PS, the semicrystalline structure is different in that the connectivity between crystalline domains seems to be enhanced, particularly for the samples with M_w = 69.6 kDa equiv PS (see Figure 3). In parts a and c of Figure 3, pi-stacked Rr-P3HT chains seem to bridge successive major crystalline lamellae. The observations by HR-TEM suggest that the boundaries between crystalline and disordered zones are less sharp than for the samples with M_w = 7.3 kDa equiv PS.

Comparing the chain packing in the crystalline lamellae vs increasing M_w reveals another striking difference between the Rr-P3HT low-M_w sample and the two samples with $M_w \geq$ 18.8 kDa equiv PS. In numerous crystalline domains of the samples with $M_w \geq$ 18.8 kDa equiv PS, we observe that successive polymer stems are shifted one with respect to the other by a more or less constant period in the direction parallel to the chain axis. As a result, the chain axis seems to be tilted with respect to the edge of the crystalline lamellae. This observation accounts for the waviness of the crystalline lamellae observed in the defocused BF TEM image (see Figure 2a). But, more importantly, it may also point at a change of fold surface with increasing M_w (vide infra).

3.2. Discussion. *3.2.a. Effect of M_w on the Interconnectivity between Crystalline Lamellae.* The general observation that charge carrier mobility in PFETs increases with increasing M_w of Rr-P3HT in conjunction with the corresponding changes in film morphology suggest that the charge transport is closely related to the film microstructure and more particularly to the semicrystalline structure of the films.[7,11,21,23−27] The results gathered in this study, (see Table 1) show that there is a marked evolution of the microstructure in the oriented thin films of Rr-P3HT as a function of increasing M_w and polydispersity of the samples. While low-M_w samples with a rather low polydispersity (1.3) yield crystalline lamellae with remarkable structural coherence and very regular lamellar thickness, samples with $M_w \geq$ 18.8 kDa equiv PS show crystalline domains with irregular shapes and strongly fluctuating lamellae. One essential conclusion gained from this study is the fact that the thickness of the crystalline lamellae, L_{cryst}, does not scale with M_w (at least in the range of investigated M_w). In fact, the observed increase of the total lamellar period, L_{lam}, (crystalline plus amorphous zones) with M_w is essentially due to the increase of the thickness of the interlamellar amorphous zones. For $M_w \geq$ 18.8 kDa equiv PS, there is a saturation of both the width of the crystalline lamellae and the amorphous interlamellar zones. The increase of M_w seems also to affect the interconnectivity between the crystalline domains. As seen in Figure 3, ordered polymer regions are observed to bridge neighboring crystalline lamellae. Tsuji and Kohjiya have observed that, for oriented films of a rather stiff-chain polymer like poly(etheretherketone) (PEEK), so-called "tie-crystallites" serve as bridging domains between adjoining major crystalline domains[40,46] (see the schematic drawing in Figure 4). Figure 3 suggests a similar situation for Rr-P3HT with high-M_w. We observe indeed that several crystalline domains are bridged via a few oriented domains of π-stacked Rr-P3HT chains.

The similarity between the crystallization of stiff-chain polymers like PEEK and the π-conjugated comb-shaped Rr-P3HT polymer seems to go beyond the role of tie-crystallites in high-M_w samples. Indeed, Waddon and co-workers have compared the crystallization of PEEK oligomers and polymers.[47] The occurrence of chain folding with increasing M_w has a drastic effect on the morphology of the PEEK crystals grown from solution. Whereas oligomers of PEEK give rise to regular lozenge-shaped crystals, irregular crystal

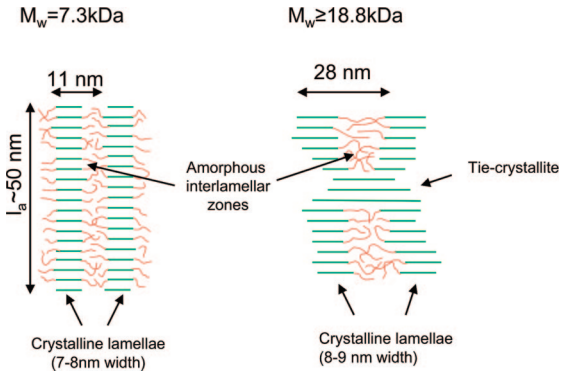

Figure 4. Schematic representation of the microstructure in semicrystalline Rr-P3HT as a function of molecular weight. The crystalline domains are shown in projection along the π-stacking direction. The chains in the crystalline lamellae are drawn in green while their sections located in the amorphous interlamellar zones appear in red.

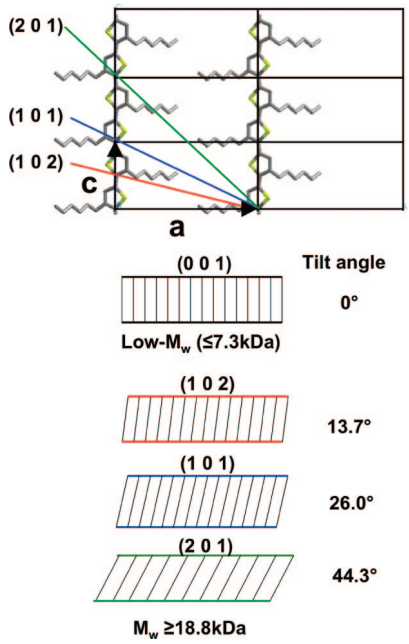

Figure 5. Illustration of different possible fold surfaces in Rr-P3HT crystalline lamellae and resulting geometries of the crystalline lamellae. The tilt angles have been calculated using the following unit cell parameters $a = 1.6$ nm and $c = 0.78$ nm.[36]

shapes are observed for the polymer crystals. Due to the chain-stiffness of PEEK, short-distance folds, as observed for polyethylene, are unlikely. As a consequence, folds span over longer distances for stiff-chain polymers like PEEK, exerting stress on the underlying crystal. This stress ultimately limits the size of the crystalline domains.

A similar explanation may be invoked to account for the very irregular lamellar morphology of Rr-P3HT for $M_w \geq 18.8$ kDa equiv PS. Moreover, the fact that, for $M_w \geq 18.8$ kDa equiv PS, the edge of the crystalline lamellae tends to make an angle with the chain direction suggests that folding exerts constraints on the packing of the chains in the crystalline lamellae. This is further manifested by the substantiated increased fluctuations of the interchain periodicity with increasing M_w (see Figure 3d). Accordingly, the tilt of the chain axis to the edge of the crystalline lamellae may be the consequence of the constrained folding of the Rr-P3HT chain.[47]

3.2.b. Effect of Molecular Weight on Folding and Fold Surfaces. The results gained by HR-TEM show a marked difference between the low-M_w sample and the samples with $M_w \geq 18.8$ kDa equiv PS in terms of chain orientation with respect to the edge of the crystalline lamellae. Since the crystalline Rr-P3HT lamellae are in edge-on orientation; i.e., the HR-TEM images correspond to the projected structure of the lamellae along the π-stacking direction (b axis), the edges of the crystalline lamellae should correspond to the fold surfaces provided P3HT can fold. For low-M_w, the edge of the lamellae is essentially perpendicular to the chain direction. This would suggest that the fold surface of the low-M_w Rr-P3HT sample is mainly the (0 0 1) plane. However, for the low-M_w sample, the probability of folding is presumably negligible given the average extended chain length (9.0 nm) with respect to the average stem length in the lamellar domains (7.5 nm).

For $M_w \geq 18.8$ kDa equiv PS, tilting of the chains in the crystalline lamellae is well-apparent both in BF and HR-TEM images (see Figure 2 and Figure 3). From a set of 50−80 crystalline lamellae, we measured the tilt angle between the chain direction and the normal to the edge of the crystalline lamellae. Interestingly, certain tilt angles occur in a statistically recurrent manner suggesting that they should be dictated by folding rules in accordance with the crystal structure of Rr-P3HT. Typical values obtained for the tilt angles are $15° \pm 3°$, $26 \pm 3°$, and $43° \pm 3°$. In Figure 5, we depict the unit cell of P3HT projected along the b axis and some possible fold surfaces. As a matter of fact, we can account for the observed experimental tilt angles by considering the following fold surfaces (1 0 2), (1 0 1), and (2 0 1). Taking a unit cell with $a = 1.6$ nm and $c = 0.78$ nm,[36] the calculated tilt angles for these fold surfaces correspond to 13.7°, 26.0°, and 44.3° respectively, in good agreement with the measured experimental values.

This result seems to support the idea that Rr-P3HT chains can fold in different crystallographic planes. A similar situation has been observed in the case of polyethylene where various fold surfaces have been observed ({0 0 1}, {1 0 1}, {2 0 1}, and{3 0 1}), depending on the crystallization conditions.[48−50] The above-mentioned sequence of fold surfaces corresponds to an increasing tilt angle, i.e., a reduced packing density of the polymer stems at the fold surface. The occurrence of different fold surfaces with relatively high tilt angles is possibly a consequence of the stress exerted by chain folding on the crystalline packing of Rr-P3HT chains.

The increasing effect of Rr-P3HT chain folding with increasing M_w on the crystalline packing of Rr-P3HT is further supported by the changes of the unit cell parameters observed in epitaxied and spin-coated thin films for Rr-P3HT of increasing molecular weight.[23,25,36] Zen et al. have observed that the interchain distance (i.e., the a parameter) tends to increase from 1.58 nm for $M_w = 3.6$ kDa equiv PS to 1.73 nm for $M_w = 36$ kDa equiv PS.[23,25] The longer the polymer chain, the larger the probability for Rr-P3HT chains to fold back into a crystalline domain, i.e., the larger the effect of chain stiffness and bulkiness on the chain packing. This result is in direct line with earlier reports on chain folding in aromatic stiff-chain polymers like PEEK showing that the interchain distance along the b axis is increased in the polymer with respect to oligomers.[47] Accordingly, in the case of Rr-P3HT, chain folding is manifested by three effects: (i) saturation of the lamellar periodicity at a value of *ca.* 28 nm, (ii) increase of the interchain distance (i.e., the a parameter), and (iii) tilting of the chains in the crystalline lamellae. Although sharp folds of Rr-P3ATs have been observed in the case of (sub)monolayers on HOPG substrates,[37,38] the new experimental evidence gained by the present HR-TEM study suggest that chain folding may also occur in 3D lamellar domains over several stem repeat periods.

4. Conclusion

HR-TEM has been used to analyze the microstructure in DES-oriented films of Rr-P3HT of three different molecular weights.

Increasing the weight-average molecular weight of Rr-P3HT from 7.3 kDa equiv PS to 69.6 kDa equiv PS results in several important structural changes. First, the structural coherence and extension of crystalline lamellae tends to decrease with increasing M_w. In particular, we observe an increase of the fluctuations of the lamellar thickness whose average value does not scale with M_w. The increase of the total lamellar periodicity is mainly related to the increase of the width of the amorphous interlamellar zones i.e. the higher the M_w of the polymer, the lower the average crystallinity in the thin films. For samples with $M_w = 69.6$ kDa equiv PS, crystalline lamellae tend to be strongly interconnected by small tie-crystallites consisting of small ordered bridging areas comprising a few π-stacked Rr-P3HT polymer chains. This enhanced connectivity may account, at least in part, for the increase in the charge carrier mobility in PFETs when the molecular weight of Rr-P3HT increases. For $M_w \geq 18.8$ kDa equiv PS, preferential tilt angles of the polymer chains in the crystalline lamellae are observed. The increasing disorder in the crystalline packing of P3HT chains in the lamellar domains, the occurrence of certain fold planes corresponding to relatively high tilt angles of the polymer chains in the crystalline lamellae and the increase of the interchain distance (i.e., the *a* axis) with increasing M_w are attributed to the effect of chain folding. The folding of comb-shaped and stiff π-conjugated Rr-P3HT chains is expected to induce stress on the chain packing and is believed to account for the increased disorder in the structure of the crystalline lamellae.

Acknowledgment. Fruitful discussions with Dr. Bernard Lotz and Dr. Marc Schmutz are gratefully acknowledged. We also thank Dr. Tony Jenkins (Merck Chemicals Ltd.) for kindly providing one of the P3HT samples used in this study.

Supporting Information Available: Figures showing the effect of Bragg filtering on the HRTEM images and a comparison of the FFTs of two HRTEM images of two P3HT films. This material is available free of charge via the Internet at http://pubs.acs.org.

References and Notes

(1) Osaka, I.; McCullough, R. D. *Acc. Chem. Res.* **2008**, *41*, 1202–1214.
(2) Leclerc, M. *J. Polym. Sci., Part A: Polym. Chem.* **2001**, *39*, 2867–2873.
(3) *Advances in Polymer Science, Polyfluorenes*; Scherf U. and Neher D. Eds., vol. *212*, Springer-Verlag: Berlin, 2008; pp 1−322.
(4) Forrest, S. R. *Nature* **2004**, *428*, 911–918.
(5) Sirringhaus, H.; Brown, P. J.; Friend, R. H.; Nielsen, M. M.; Bechgaard, K.; Langeveld-Voss, B. M. W.; Spiering, A. J. H.; Janssen, R. A. J.; Meijer, E. W.; Herwig, P.; de Leeuw, D. M. *Nature* **1999**, *401*, 685–688.
(6) Sirringhaus, H. *Adv. Mater.* **2005**, *17*, 2411–2425.
(7) Salleo, A. *Mater. Today* **2007**, *10*, 38–45.
(8) Allard, S.; Forster, M.; Souharce, B.; Thiem, H.; Scherf, U. *Angew. Chem., Int. Ed.* **2008**, *47*, 2–31.
(9) Chabinyc, M. L. *J. Vac. Sci. Technol. B* **2008**, *26*, 445–457.
(10) Ong, B. S.; Wu, Y.; Li, Y.; Liu, P.; Pan, H. *Chem. Eur. J.* **2008**, *14*, 4766–4778.
(11) Chabinyc, M. L.; Jimison, L. H.; Rivnay, J.; Salleo, A. *MRS Bull.* **2008**, *33*, 683–689.
(12) Ma, W.; Yang, C.; Gong, X.; Lee, K.; Heeger, A. J. *Adv. Funct. Mater.* **2005**, *15*, 1617–1622.
(13) Mayer, A. C.; Scully, S. R.; Hardin, B. E.; Rowell, M. W.; McGehee, M. D. *Mater. Today* **2007**, *10*, 28–33.
(14) Kim, J. Y.; Lee, K.; Coates, N. E.; Moses, D.; Nguyen, T.-Q.; Dante, M.; Heeger, A. J. *Science* **2007**, *317*, 222–225.
(15) Bundgaard, E.; Krebs, F. C. *Sol. Energy Mater. Sol. Cells* **2007**, *91*, 954–985.
(16) Cravino, A. *Polym. Int.* **2007**, *56*, 943–956.
(17) Hoppe, H.; Sariciftci, N. S. *Advances in Polymer Science*; Marder S. R., Lee K.-S., Eds.; Springer-Verlag: Berlin, 2008; Vol. *214*, pp 1−86.
(18) Thompson, B. C.; Fréchet, J. M. J. *Angew. Chem., Int. Ed.* **2008**, *47*, 58–77.
(19) Brabec, C. J.; Durrant, J. R. *MRS Bull.* **2008**, *33*, 670–675.
(20) Moore, J. S. *J. Am. Chem. Soc.* **2008**, *130*, 12201–12203.
(21) Verilhac, J. M.; LeBlevennec, G.; Djurado, D.; Rieutord, F.; Chouiki, M.; Travers, J.-P.; Pron, A. *Synth. Met.* **2006**, *156*, 815–823.
(22) Anthony, J. E.; Heeney, M.; Ong, B. S. *MRS Bull.* **2008**, *33*, 698–705.
(23) Zen, A.; Pflaum, J.; Hirschmann, S.; Zhuang, W.; Jaiser, F.; Asawapirom, U.; Rabe, J. P.; Scherf, U.; Neher, D. *Adv. Funct. Mater.* **2004**, *14*, 757–764.
(24) Kline, R. J.; McGehee, M. D.; Kadnikova, E. N.; Liu, J.; Fréchet, J. M. J.; Toney, M. F. *Macromolecules* **2005**, *38*, 3312–3319.
(25) Zen, A.; Saphiannikova, M.; Neher, D.; Grenzer, J.; Grigorian, S.; Pietsch, U.; Asawapirom, U.; Janietz, S.; Scherf, U.; Lieberwirth, I.; Wegner, G. *Macromolecules* **2006**, *39*, 2162–2171.
(26) Zhang, R.; Li, B.; Iovu, M. C.; Jefferies-EL, M.; Sauvé, G.; Cooper, J.; Jia, S.; Tristram-Nagle, S.; Smilgies, D. L.; Lambeth, D. N.; McCullough, R. D.; Kowalewsky, T. *J. Am. Chem. Soc.* **2006**, *128*, 3480–3481.
(27) Joshi, S.; Grigorian, S.; Pietsch, U.; Pingel, P.; Zen, A.; Neher, D.; Scherf, U. *Macromolecules* **2008**, *41*, 6800–6808.
(28) Chang, J.-F.; Sun, B.; Breiby, D. W.; Nielsen, M. N.; Sölling, T. I.; Giles, M.; McCulloch, I.; Sirringhaus, H. *Chem. Mater.* **2004**, *16*, 4772–4776.
(29) Yang, H.; Shine, T. J.; Yang, L.; Cho, K.; Ryu, C. Y.; Bao, Z. *Adv. Funct. Mater.* **2005**, *15*, 671–676.
(30) Lu, G.; Li, L.; Yang, X. *Adv. Mater.* **2007**, *19*, 3594–3598.
(31) Kline, R. J.; McGehee, M. D.; Toney, M. F. *Nat. Mater.* **2006**, *5*, 222–228.
(32) Park, Y. D.; Lim, J. A.; Lee, H. S.; Cho, K. *Mater. Today* **2007**, *10*, 46–54.
(33) Ho, P. K.-H.; Chua, L.-L.; Dipankar, M.; Gao, X.; Qi, D.; Wee, A. T.-S.; Chang, J.-F.; Friend, R. H. *Adv. Mater.* **2007**, *19*, 215–221.
(34) Han, C. H.; Bhattacharya, A.; Di Ventra, M.; Eckenstein, J. N.; Frisbie, C. D.; Gershenson, M. E.; Goldman, A. M.; Inoue, I. H.; Mannhart, J.; Millis, A. J.; Morpurgo, A. F.; Natelson, D.; Triscone, J.-M. *Rev. Mod. Phys.* **2006**, *78*, 1185–1212.
(35) Brinkmann, M.; Wittmann, J.-C. *Adv. Mater.* **2006**, *18*, 860–863.
(36) Brinkmann, M.; Rannou, P. *Adv. Funct. Mater.* **2007**, *17*, 101–108.
(37) Mena-Osteriz, E.; Meyer, A.; Langeveld-Voss, B. M. W.; Janssen, R. A. J.; Meijer, E. W.; Bäuerle, P. *Angew. Chem., Int. Ed.* **2000**, *39*, 2679–2684.
(38) Grévin, B.; Rannou, P.; Payerne, R.; Pron, A.; Travers, J.-P. *J. Chem. Phys.* **2003**, *118*, 7097–7102.
(39) Kobayashi, T. *Crystals: growth, properties and applications*; Springer-Verlag: Berlin, 1991; p 263.
(40) Tsuji, M.; Kohjiya, S. *Prog. Polym. Sci.* **1995**, *20*, 259–308.
(41) Liu, J.; Loewe, R. S.; McCullough, R. D. *Macromolecules* **1999**, *32*, 5777–5785.
(42) Pradère, P.; Thomas, E. L. *Ultramicroscopy* **1990**, *32*, 149–168.
(43) Here the term "edge-on" refers to the orientation of the crystalline lamella on the TCB substrate. This orientation is distinct from the "face-on" orientation which is often found in the literature to refer to the orientation of P3HT chains lying with their conjugated backbone down on the substrate.
(44) The tentative packing of the Rr-P3HT depicted in Figure 1c has been obtained from the simulation of the selected area electron diffraction (SAED) pattern in ref 36 and the oriented fiber pattern in ref 35. The details of this simulation will be reported elsewhere.
(45) Gonzàlez-Ronda, L.; Martin, D. C. *Macromolecules* **2004**, *37*, 2872.
(46) Kawamura, H.; Tsuji, M.; Kawaguchi, A.; Katayama, K. *Bull. Chem. Res., Kyoto Univ.* **1990**, *68*, 41.
(47) Waddon, A. J.; Keller, A.; Blundell, D. J. *Polymer* **1992**, *33*, 27.
(48) Wunderlich, B. *Structure, Morphology, Defects in Macromolecular Physics*; Academic Press: London 1973; Vol. *1*.
(49) Lotz, B.; Wittmann, J.-C. *Materials Science and Technology: a comprehensive treatment*; Wiley: Weinheim, Germany, 1993.
(50) Guttman, C. M.; DiMarzio, E. A.; Hoffman, J. D. *Polymer* **1981**, *22*, 597.

MA8023415